Int. J. Electrochem. Sci., 14 **(2019)** 6000 – 6008, doi: 10.20964/2019.07.37

International Journal of
ELECTROCHEMICAL
SCIENCE
www.electrochemsci.org

$MnSe_2$/Se Composite Nanobelts as an Improved Performance Anode for Lithium Storage

Xiantao Shang[1], *Shuo Li*[2], *Kai Wang*[2], *Xiaoling Teng*[1], *Xia Wang*[1], *Qiang Li*[1,*], *JinBo Pang*[3], *Jie Xu*[1], *Derang Cao*[1], *Shandong Li*[1,*]

[1] College of Physics Science, University-Industry Joint Center for Ocean Observation and Broadband Communication, Qingdao University, No.308 Ningxia Road, Qingdao, 266071, China
[2] College of Electrical Engineering, Qingdao university, No.308 Ningxia Road, Qingdao, 266000, China
[3] Shandong Collaborative Innovation Center of Technology and Equipements for Biological Diagnosis and Therapy, Institute for Advanced Interdisciplinary Research (iAIR), University of Jinan, Jinan, 250022, China
[*]E-mail: liqiang@qdu.edu.cn, lishd@qdu.edu.cn

Received: 4 April 2019 / *Accepted:* 7 May 2019 / *Published:* 10 June 2019

$MnSe_2$/Se composite nanobelts which are used as a kind of the anode electrode material in lithium-ion batteries have been prepared by a straightforward method of the hydrothermal synthesis, and their morphologies, structures and electrochemical performances have been investigated. The prepared nanocomposition exhibits the excellent rate performance and the excellent electrochemical performance, such as the good cycling stability (572 mAh g^{-1} at current density of 200 mA g^{-1} after 200 cycles). The improved performance of the electrochemical lithium storage should be attributed to the architecture and the component of composite nanobelts, which could depress the pulverization and enhance the electrical conductivity. Our results indicate that the $MnSe_2$/Se composite nanobelts have potential applications prospect in high-performance lithium-ion batteries.

Keywords: Lithium-ion batteries; Anode; $MnSe_2$/Se composite; Hydrothermal synthesis

1. INTRODUCTION

In the past few decades, the high-performance electrode materials in lithium-ion batteries (LIBs) had attracted significant interest due to their tremendous value in the application of portable electronics, electric vehicles, the power grids, the high-voltage alternating current (HVAC) system and even the nanobubbles adsorbed on the surface of hydrophobic particles [1-4]. Until now, various materials have been widely explored as anodes based on different energy storage mechanisms such as intercalation,

alloying, conversion reactions and the frequency modulation technology [2, 5]. As the main members of electrochemical reactions modes, the transition metal chalcogenides (TMC) has the capacities which are several times higher than those of insertion-type anode [6, 7]. Like the hydrophobic carbon nanotubes [8], TMC is considered as a kind of attractive anode material for lithium-ion batteries. Recently, the metal selenides (MSe) have been attracting significant attentions due to their narrow band gap with good conductivity [9]. However, the large volume expansion with pulverization of these materials during electrochemical reactions still limites cycling and rate performances. Not only that, but also the ensembles, the ligand, and the strain in the close-packed surfaces affect the conductivity of materials [10]. The oxygen reduction reaction (ORR) of metals (such as Pd and Rh) also affects the electrical conductivity of metals [11, 12].

To overcome the intrinsic drawbacks in the cycling and rate performances, many kinds of measures have been developed, including the following aspects:

(1) Fabricating the materials of the carbide, the phosphorus and the nanostructured transition metal selenides, such as the porous carbons [13], the nanoplates [14], nanospheres [15], and the nanoparticles [16], which can replace the materials of the TMC.

(2) Various novel materials have been produced in the last three years. [17] provides a kind of material that is named as "MXenes", and the MXenes has the extraordinary electrochemical and optoelectronic properties in lithium-ion batteries. [18] proposes the concept of the "single-walled carbon nanotubes (SWNT)", which has the more effectual electrostatic field than the perpendicular. Besides, Pang *et al* uses a facile confinement chemical vapor deposition approach in which they simply "sandwich" two Si wafers with their oxide faces in contact to form uniform monolayer graphene, which has the high conductivity [19]. Furthermore, phosphorene and black phosphorus possess greater potential for high electrochemical performance [20]. What's more, a series of stable metal–organic zeolites (H-MOZs) which are fabricated rapidly by a novel and transferable approach significantly enhances the rate performances of the materials [21].

(3) Using catalysts can also increase the rate of ORR, which could enhance the performance during the period of charging-discharging in batteries. The Na_2SiO_3 and the conductive carbon black used as the catalysts have the same effect as the mixture of electrochemical oxidation-peroxydisulfate (PDS/EO) in increasing the rate of ORR [22, 23].

Among these materials provided in many methods, manganese-based compounds have been utilized as promising anode materials in the high-performance LIBs due to the Mn's abundance, relative low cost, low toxicity and good performance in storage systems [24, 25]. Li *et al* fabricated MnSe nanocubes with superior lithium storage properties [26]. Liu *et al* also achieved excellent cycle stability and high rate capacity in MnSeN-doped carbon double nanotubes [27]. However, to the best of our knowledge, the synthesis of nanostructured $MnSe_2$ anode materials for energy storage has not been reported. In this work, $MnSe_2$/Se composite nanobelts are synthesized in one step by hydrothermal method. As a kind of the anode material, they deliver a high reversible capacity of 572 mAh g^{-1} at the current density of 200 mA g^{-1} after 200 cycles and show a good rate performance. The improved lithium storage performance can be related to the composite nanobelts architecture and component, which could depress the pulverization and enhance the electrical conductivity.

2. EXPERIMENTAL

The preparation process of the $MnSe_2$/Se composite nanobelts is shown in Figure.1. Firstly, 1.5 mmol of manganese acetate tetrahydrate and 1.5 mL of acetic acid were dissolved in 5 mL of the deionized water at the room temperature. Secondly, 10 mL of freshly prepared NaHSe solution (0.15 M, configuration by the Klaymen method [28]) and 2 mL of 80 wt% hydrazine monohydrate were added into the solution obtained in the first step. The pH of the mixed solution was adjusted by using the sodium hydroxide solution with a concentration of 1 mol/L and the acetic acid solution with a concentration of 1 mol/L. Thirdly, the mixture was transferred into a Teflon-lined autoclave which had the capacity of 60 ml. At last, the Teflon-lined autoclave had been sealed and maintained at 180°C for 12 h and then cooled them to the room temperature.

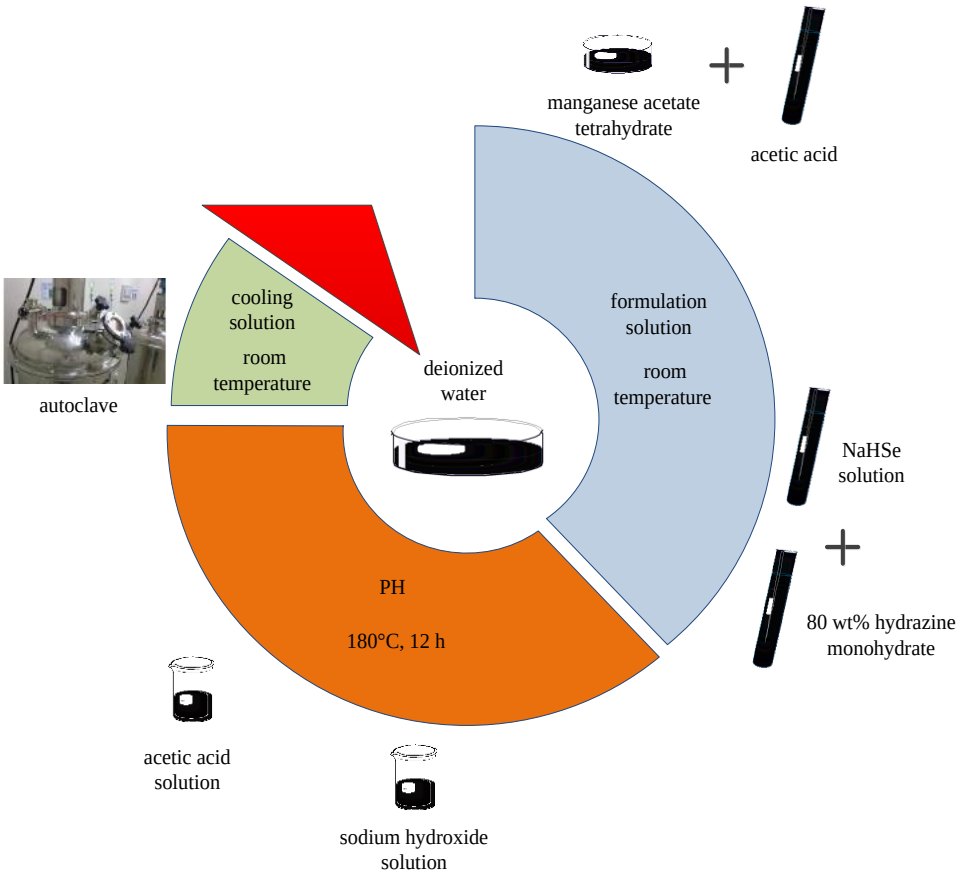

Figure 1. The preparation process of the $MnSe_2$/Se composite nanobelts.

The as-prepared samples were characterized with X-ray diffractometer (Rigaku D/Max), X-ray photoelectron spectroscopy (Thermo Scientific ESCALAB 250XI), scanning electron microscopy (JSM-6700F), and transmission electron microscopy (TEM,JEM-2100).

Electrochemical experiments were performed with the CR-2032-type coin cells, which were assembled inside an argon-filled glove box with a lithium foil as counter and a Celgard 2250 polypropylene film as separator. The electrolyte solution had a type of the standard electrolyte which

was prepared according to the ratio that ethylenecarbonate (EC)/propylene carbonate (PC)/dimethyl carbonate (DMC)/$LiPF_6$ equaled to 1:1:1:1. Galvanostatic cycling measurements were conducted by a LAND-ct2001A battery system. Electrochemical impedance was obtained on an electrochemical workstation (CHI660E).

3. RESULTS AND DISCUSSION

Fig.2(a) shows an XRD pattern of the as-synthesized sample. It can be obviously that all of the diffraction peaks can be well assigned to $MnSe_2$ [PDF card No. 65-3336] and Se [PDF card No. 06-0362], indicating that the as-synthe sized sample is a mixture of Se phases and $MnSe_2$ phases.

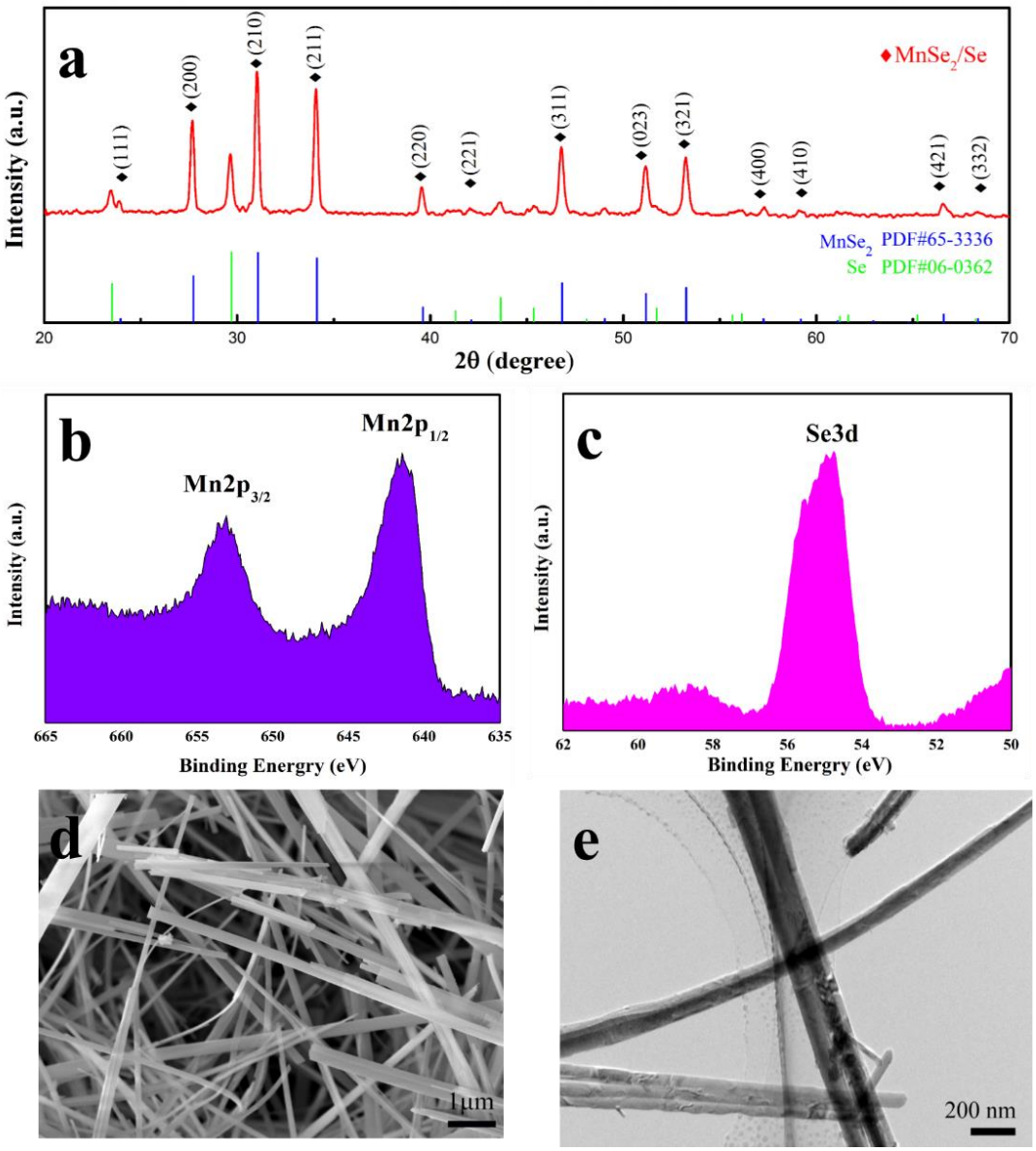

Figure 2. (a) XRD patterns; (b, c) XPS survey spectra; (d) SEM; (e) TEM images of the prepared $MnSe_2$/Se composites.

Moreover, XPS is performed to characterize the chemical states of Mn and Se in the prepared samples, as displayed in Fig.2(b) and Fig.2(c). The Mn2p peaks in Fig.2(b) are fitted to two obvious characteristic peaks of $Mn_{1/2}$ and $Mn2p_{3/2}$ respectively, responding to Mn^{2+} accorded with the previous reports [29]. As shown in Fig.2(c), the peak at 54.7 eV in the 3d spectrum of the Se indicates the existence of Se_2^{2-}, and the asymmetry of the peak at 55.3 eV can be related to the presence of a small amount of selenium [30]. The morphology of the sample is observed by using SEM and TEM , whose images are showed in Fig.2(d) and Fig.2(e) respectively. The as-prepared sample shows a long beltlike morphology which has the width of a few hundreds nanometers and the length of several tens of micrometers.

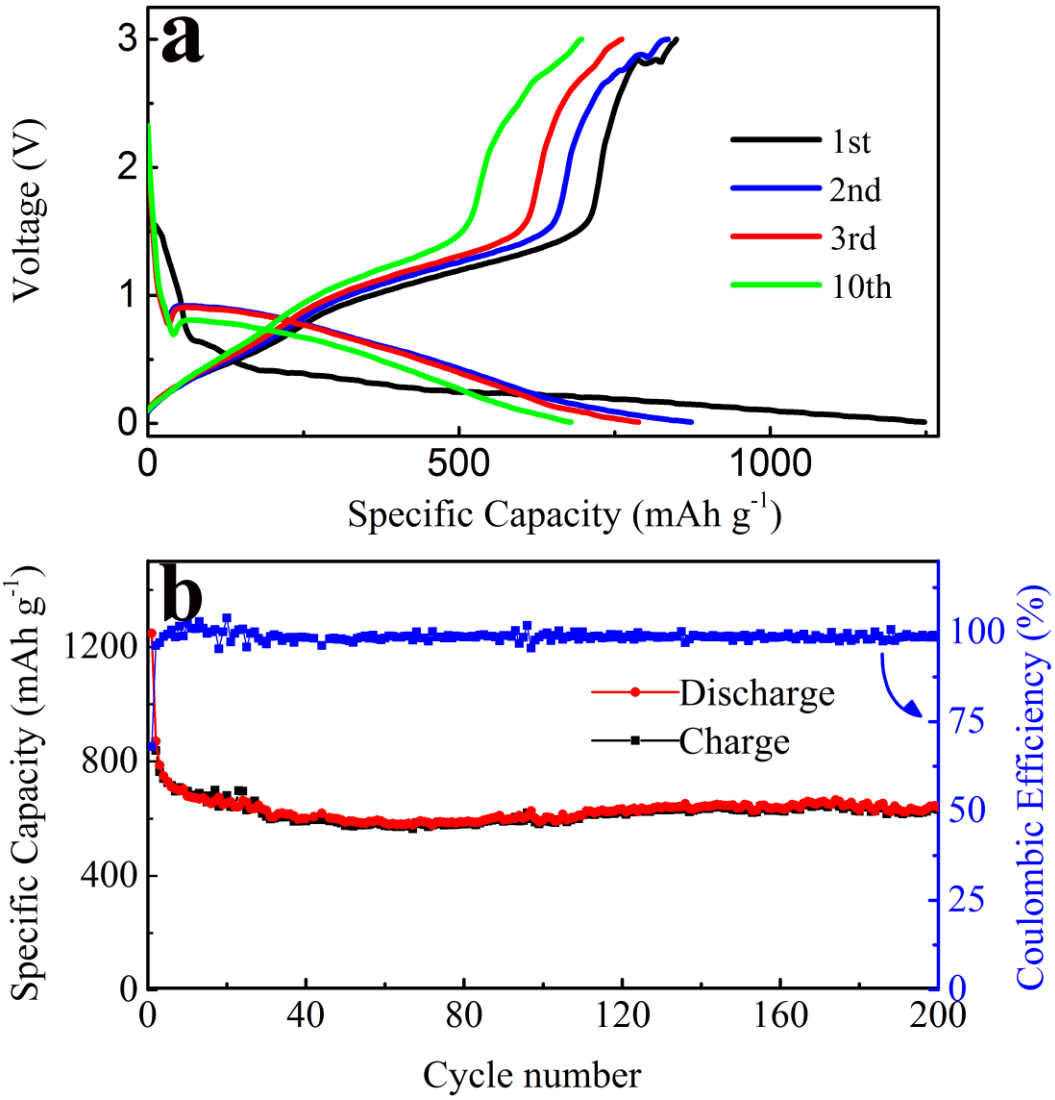

Figure 3. (a) Charge and discharge voltage profiles. (b) Cycling performance and the corresponding Coulombic efficiency.

The electrochemical properties of the prepared samples as LIB anode materials were carried out in CR 2032 coin cells. Fig.3(a) shows the discharge-charge voltage curve for $MnSe_2$/Se with a circulating

current density of 200 mA g^{-1} in the 1st cycle, the 2nd cycle and the 10th cycle respectively. In the first cycle, the $MnSe_2$/Se electrode shows a discharge capacity of 1247.7 mAh g^{-1} as well as a charge capacity of 851.9 mAh g^{-1}, and the percentage of the Coulomb efficiency in the $MnSe_2$/Se electrode is 68.2%, which is attributable to the formation of solid electrolyte interface layer (SEI) during the period of discharging. The cycle performance curve of $MnSe_2$/Se as shown in Fig.3(b) was also tested at the same current density of 200 mA g^{-1}. It can be seen that the reversible capacity gradually decreases to around 600 mAh g^{-1} after 30 cycles and keeps stable in the following cycles, exhibiting a capacity of 572 mAh g^{-1} after 200 cycles.

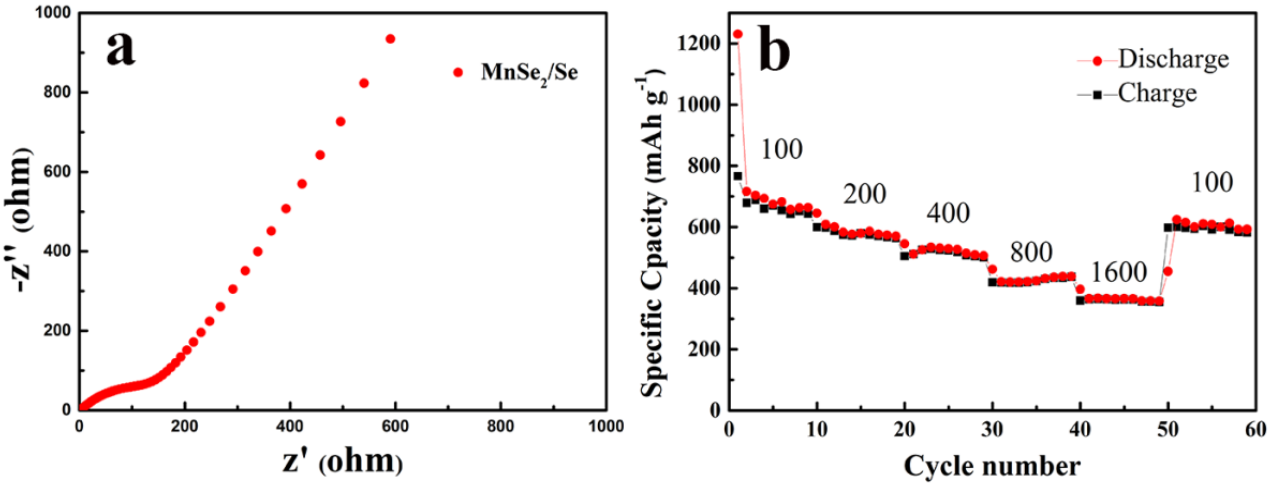

Figure 4. (a) EIS of the nanocrystalline $MnSe_2$/Se composite nanobelts. (b) Rate capability at various current densities from 100 mA g^{-1} to 1600mA g^{-1}

Moreover, measuring the MnSe2/Se electrode which is performed in Fig.4(a) by using the electrochemical impedance spectra (EIS) in order to investigate the Li^+ transfer behavior. The overall interface resistance is as low as 130 Ω, which can be deduced from the single semicircle in the high-middle frequency. As shown in Fig.4(b), the good conductivity of $MnSe_2$/Se nanobelts causes the good performance of the rate capability. A reversible capacity of 366.5 mAh g^{-1} can still be delivered at the current density of 1600 mA g^{-1}, which is corresponding to 54.9% of the retention of the capacity at the current density of 100 mA g^{-1}. More importantly, when the specific current reduces to 100 mA g^{-1}, the reversible lithium capacity could recover to its original capacity which is nearly 620 mAh g^{-1}. The excellent performance of the rate may benefits from the existence of the component of the selenium, since some previous papers show that Fe_2O_3/Se composite nanorods [34] and NiO/Se nanocomposites [35] also exhibit the improved rate performances.

The comparison of the two kinds of electrode materials made of Manganese compounds is shown in the Table 1. Compared with the other MnSe nanostructures reported previously in [29], which is named as “high-quality cubic phase α-MnSe nanocubes (MS1)”, the material in this paper has the better cycling stability (such as the reversible capacity and the Coulomb efficiency). This good cycling stability

can be attributed to the nanobelts architecture of $MnSe_2$/Se, which can not only shorten the lithium ions diffusion distance but also buffer volume changes [31-33].

Table 1. The comparison between the two kinds of electrode materials made of Manganese compounds

Anode materials	Charge capacity[a] (mAh g^{-1})	Discharge capacity[a] (mAh g^{-1})	Coulomb efficiency[a]	Reversible capacity[b] (mAh g^{-1})	Ref
$MnSe_2$/Se composite nanobelts	851.9	1247.7	68.2%	572	This work
high-quality cubic phase α-MnSe nanocubes (MS1)	401	790	50.8%	320	29

[a]The data collected from the first cycle
[b]The data after 200 cycles

4. CONCLUSION

In summary, $MnSe_2$/Se composite nanobelts have been successfully prepared by the one-step hydrothermal method and exhibited a kind of good cycling stability (572 mAh g^{-1} of the reversible capacity at 200 mA g^{-1} of the current density after 200 cycles). The $MnSe_2$/Se composite nanobelts shows the excellent rate performance when it works as the material of the anode electrode in lithium-ion batteries. Such high electrochemical performance can be attributed to the architecture of nanobelts and the component of the selenium, which could depress the pulverization and enhance the electrical conductivity. Our results indicate that the $MnSe_2$/Se composite nanobelts have potential applications in high-performance LIBs.

ACKNOWLEDGMENTS
This work was supported partly by the National Natural Science Foundation of China [11504192, 11604172, 11674187, 11704211]; the National Science Foundation of Shandong Province [BSB2014010, ZR2018BEM012]; Science and Technology Board of Qingdao [16-5-1-2-jch, 18-2-2-7-jch].

References

1. J. M. Tarascon and M. Armand, *Nature*, 414 (2001) 359.
2. C. Zhu, R. E. Usiskin, Y. Yu and J. Maier, *Science*, 358 (2017) 2808.
3. L. C. Wu, Y. Han, Q. R. Zhang and S. Zhao, *RSC Advances*, 9 (2019) 1792.
4. J. L. Wang, L. H. Tang, L. Y. Zhao and Z. E. Zhang, *Energy* , 172 (2019) 1066.

5. K. Wang, L. W. Li, Y. Lan, P. Dong and G.T. Xia, *Mathematical Problems in Engineering*, (5) (2019) (1).
6. Y. Qin, L. Qiang, X. Jie, W. Xia, G. Zhao, C. Liu, Y. Xu, Y. Long, S. Yan and S. Li, *Electrochimica Acta*, 224 (2017) 90.
7. J. Dai, J. Li, Q. Zhang, M. Liao, T. Duan and W. Yao, *Materials Letters*, 236 (2019) 483.
8. K. Wang, J. B. Pang, L. W. Li, S. Z. Zhou, Y. H. Li and T. Z. Zhang, *Frontiers of Chemical Science and Engineering*, 12 (2018) 376.
9. Z. Ali, M. Asif, X. Huang, T. Tang and Y. Hou, *Advanced Materials*, 2 (2018) 1802745.
10. H. Li, K. Shin and G. Henkelman, *The Journal of Chemical Physics*, 149 (2018) 1.
11. H. Li, L. Luo, P. Kunal, C. S. Bonifacio, Z. Y. Duan, J. C. Yang, S. M. Humphrey, R. M. Crooks and G. Henkelman, *The Journal of Physical Chemistry* C, 122 (2018) 2712.
12. H. Li and G. Henkelman, *The Journal of Physical Chemistry* C, 121 (2017) 27504.
13. K. Wang, S. Z. Zhou, Y. T. Zhou, J. Ren, L. W. Li and Y. Lan, *International Journal of Electrochemical Science*, 13 (2018) 10766.
14. Z. Zhou, W. Zhang, W. Zhao, Z. Yang and C. Zeng, *Journal of Electronic Materials*, 43 (2013) 359.
15. P. Ge, S. Li, L. Xu, K. Zou, X. Gao, X. Cao, G. Zou, H. Hou and X. Ji, *Advanced Energy Materials*, 9 (2019) 1803035.
16. H. Wang, X. Wang, Q. Li, H. Li, J. Xu, X. Li, H. Zhao, Y. Tang, G. Zhao, H. Li, H. Zhao and S. Li, *ACS Applied Materials & Interfaces*, 10 (2018) 38862.
17. J. B. Pang, Mendes, R. G. Bachmatiuk, A. Zhao, L. Ta, H. Q. Gemming, T. H. Liu, Z. Liu and M. H. Rummeli, *Chem. Soc. Rev*, 48 (2019) 72.
18. Q. R. Zhang, Y. Han, L. C. Wu, *Chemical Engineering Journal*, 363 (2019) 278.
19. J. B. Pang, R. G. Mendes, P. S. Wrobel, M. D. Wlodarski, H. Q. Ta, L. Zhao, L. Giebeler, B. Trzebicka, T. Gemming, L. Fu, Z. F. Liu, J. Eckert, A. Bachmatiuk and M. H. Rummeli, ACS Nano, 11 (2017) 1946.
20. J. B. Pang, A. Bachmatiuk, Y. Yin, B. Trzebicka, L. Zhao, L. Fu, R. G. Mendes, T. Gemming, Z. F. Liu and M. H. Rummeli, *Advanced Energy Materials*, 8 (2018) 1.
21. C. X. Duan, F. E. Li, M. H. Yang, H. Zhang, Y. Wu and H. X. Xi, *Ind. Eng. Chem. Res*, 57 (2018) 15385.
22. L. Kang, H. L. Du, X. Du, H. T. Wang, W. L. Ma, M. L. Wang and F. B. Zhang, *Desalination and Water Treatment*, 125 (2018) 296.
23. X. Li, S. F. Tang, D. L. Yuan, J. C. Tang, C. Zhang, N. Li and Y. D. Rao, *Ecotoxicology and Environmental Safety*, 177 (2019) 77.
24. Y. Chu, L. Guo, B. Xi, Z. Feng, F. Wu, Y. Lin, J. Liu, D. Sun, J. Feng, Y. Qian and S. Xiong, *Advanced Materials*, 30 (2018) 1704244.
25. K. Wang, L. W. Li, W. Xue, S. Z. Zhou, Y. Lan, H. W. Zhang and Z. Q. Sui, *International Journal of Electrochemical Science*, 12(2017) 8306.
26. P. Ge, C. Zhang, H. Hou, B. Wu, L. Zhou, S. Li, T. Wu, J. Hu, L. Mai and X. Ji, *Nano Energy*, 48 (2018) 617.
27. D. H. Liu, W. H. Li, H. J. Liang, H. Y. Lü, J. Z. Guo, J. Wang and X. L. Wu, *Journal of Materials Chemistry* A, 6 (2018) 15797.
28. D. L. Klayman and T. S. Griffin, *Journal of the American Chemical Society*, 95 (1973) 9111.
29. N. Li, Y. Zhang, H. Y. Zhao, Z. Q. Liu, X.Y. Zhang and Y. P. Du, *Inorganic Chemistry*, 55 (2016) 2765.
30. T. Qin, J. Lu, S. Wei, P. Qi, Y. Peng, Z. Yang and Y. Qian, *Inorganic Chemistry Communications*, 5 (2002) 369.
31. H. C. Park, K. H. Lee, Y. W. Lee, S. J. Kim, D. M. Kim, M. C. Kim and K. W. Park, *Journal of Power Sources*, 269 (2014) 534.
32. L. L. Xing, C. X. Cui, B. He, Y. X. Nie, P. Deng and X. Y. Xue, *Materials Letters*, 96 (2013) 158.

33. J. Li, Q. Sun, Z. Wang, J. Xiang, B. Zhao, Y. Qu and B. Xiang, *Applied Surface Science*, 412 (2017) 113.
34. J. S. Cho, J. S. Park, K. M. Jeon and Y. C. Kang, *Journal of Materials Chemistry* A, 5 (2017) 10632.
35. X. Li, Y. Xiang, B. Qu and S. Su, *Materials Letters*, 203 (2017) 1.